ACS OMEGA

Article

http://pubs.acs.org/journal/acsodf

Probing Stress-Induced Optical Birefringence of Glassy Polymers by Whispering Gallery Modes Light Localization

Karolina Milenko,[†] Stavros Pissadakis,[*,†] Georgios Gkantzounis,[∥] Alina Aluculesei,[†] and George Fytas[*,†,‡,§]

[†]Foundation for Research and Technology-Hellas (FORTH), Institute of Electronic Structure and Laser (IESL), N. Plastira 100, Heraklion 70013, Greece

[‡]Department of Materials Science, University of Crete, Heraklion 71003, Greece

[§]Max Planck Institute for Polymer Research, Ackermannweg 10, 55128 Mainz, Germany

[∥]Department of Physics, Advanced Technology Institute, University of Surrey, GU2 7XH Guildford, U.K.

Supporting Information

ABSTRACT: An optical resonance method for the determination of the strain- and stress-optical coefficients of optically transparent polymers is presented and exemplified for monodisperse and bidisperse molecular weight polystyrene (PS). This method employs whispering gallery modes (WGMs) resonation inside a spheroid polymeric cavity, suspended on an optical fiber taper waist, which, in turn, is used for subjecting the polymeric resonator to controlled strain conditions. The wavelength shifts of equal order transverse electric and transverse magnetic polarization WGMs are measured, as well as their relative birefringence versus applied strain. For monodisperse PS microspheroids (2 and 50 kDa) the stress-optical coefficient is negative, contrary to the results for bulk PS in the glassy state indicating different phenyl group orientation of the PS monomer with respect to the strain direction. In the bidisperse (2 and 50 kDa) spheroid with a symmetric monomer composition, local structural irregularities are probably responsible for the observed coupling between WGMs. The method possesses metrological capabilities for probing the molecular orientation of polymer-based resonators.

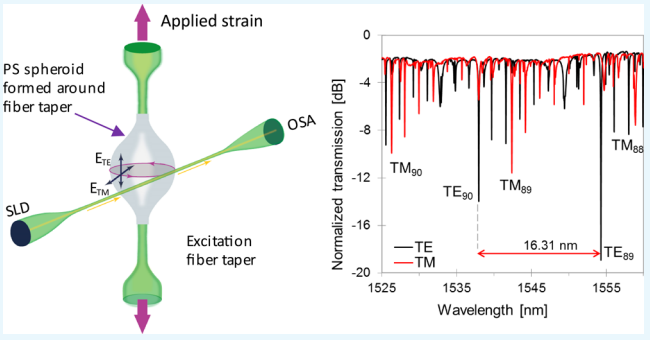

INTRODUCTION

Whispering gallery mode (WGM) light localization into spherical symmetry resonators is a powerful tool for the development of photonic devices for sensing,[1] lasing,[2] and spectroscopic[3] applications. The spectral signature of light localization by WGMs is directly related to the optogeometrical characteristics of the resonating cavity by means of its refractive index ellipsoid, loss, and geometry. The light localization by WGMs through an iterative round-trip resonation into a closed spherical cavity renders the spectral behavior of this system impressively sensitive to spatially confined modifications of its physical properties, as long as these modifications overlap with the modal volume of the WGMs. Their confinement through total internal reflection occurs along the interface of the cavity surface with the outer environment that enhances the surface sensitivity of the WGMs.

There are several examples wherein WGM light localization has been utilized for developing light localization, sensing, propulsion, and optomechanical oscillation devices, whereas resonant cavities are constituted from hard (glasses, crystals)[4] or soft (polymer) optical materials.[5] Specific stimulation schemes have been applied for modifying the optogeometrical characteristics of WGM spheroidal cavities by means of mechanical actuation (compression and stretching[6]) or application of electrical field[7] for tuning the shape and/or the refractive index of the resonator. Beyond the previous, material science can also benefit from these superior light circulation and interrogation features for detecting, for example, "near surface" phenomena. Specifically, polymers exhibit interesting optical, mechanical, and rheological properties, which classify them as key role materials in the fields of photonics, chemistry, and biotechnology; moreover, the polymer behavior under confinement remains an important and challenging task.[8] Thus, spatially confined thermomechanical, rheological, or chemical processes on the nanoscale[9] can be potentially traced and monitored, as long as they exhibit a direct signature into the optical properties of the WGM resonation cavity. "Soft" WGM resonators have been presented using polystyrene (PS),[10] poly(dimethylsiloxane),[11] and other polymers,[12] mostly attaining modal tunability using mechanical strain or temperature stimulus. However, all of this work is aimed at understanding the WGM resonance manipulation utilizing external stimula-

Received: September 21, 2017
Accepted: November 3, 2017
Published: December 20, 2017

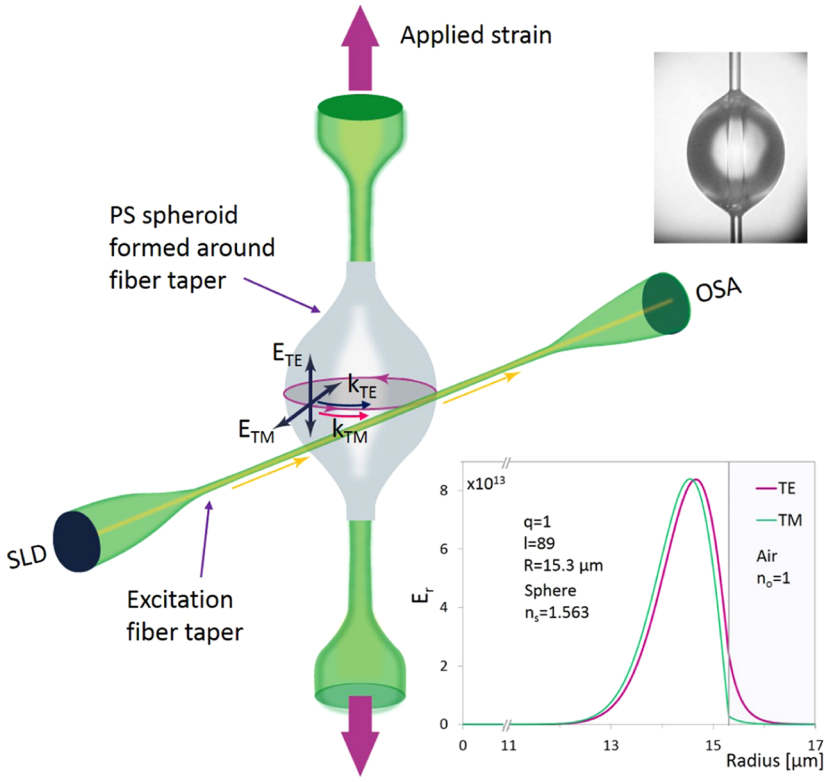

Figure 1. Configuration of the polystyrene (PS) resonator and whispering gallery mode (WGM) excitation with TE and TM polarization using a broadband superluminescent laser diode (SLD) and optical spectrum analyzer (OSA) for signal recording. The strain is applied at both fiber taper ends through controllable fiber elongation. TE and TM WGM mode field distributions in the resonator (low inset) and an image of a 30.6 μm diameter PS spheroid, fabricated around the fiber taper (upper inset).

tions, which is a precondition to exploit novel photonic devices applications. On the contrary, there are few results that solely focus on the use of soft matter WGM optical cavities for the study of the mechanical and photoelastic properties of the polymeric material.[13]

The principal motivation of the present work is to access fundamental polymer physics questions at the microscale by tracing optical quantities utilizing mechanically tuned WGM resonators as a primary transducing scheme. We realize a versatile configuration of polymer microspheroidal WGM resonators supported on a thin optical silica fiber taper (Figure 1 inset) for a straightforward study of the photoelastic properties of the material constituting the resonating cavity. This thin optical fiber scheme allows the controllable application of minimal strains along the longitudinal axis of the supporting microfiber onto the cavity, thus warranting linear material response. Irrespective of the cavity material, the light localization through WGMs inside the spheroid cavity exhibits inherent polarization sensitivity.[14] Yet, the field amplitudes of the two polarization components (transverse electric (TE) and transverse magnetic (TM) in Figure 1) are subject to strain-related walk-off paths associated with the material local structure. The photoelasticity of polymers quantified by the stress-optical coefficient depends on the collective segmental and chain orientation, which, in turn, is related to the physical state of the polymer. For the well-studied amorphous polystyrene (PS), this coefficient is distinct in the glassy ($k > 0$) and the rubber ($k < 0$) state above the glass transition.[15] The results of the present photonic method for glassy mono- and bidisperse PS microspheroids using low- and high-molecular-weight PS point out that elasto-optic response can substantially deviate from the bulk behavior when interfacial effects and internal stresses become important. Compensation and control of polymer birefringence is important for polymer-based photonics.[16]

Photoelasticity relies on the differential optical path of orthogonal polarization states of light traveling along the stress-loaded bulk optical species. Usually, interferometric fringe shifting methods are used for tracing phase differences and then evaluate the photoelastic coefficient for the investigated sample.[17] In the configuration of the WGM spheroid scheme of Figure 1, the small strain simultaneously modifies the refractive index and the shape/size of the attached polymeric WGM cavity. This combined optogeometrical perturbation results in clear and repeatable spectral changes in the WGM signature. The spectral notches of the WGMs localized inside the polymeric spheroid are spectrally shifted versus the applied strain, with the spectral shifts being different for WGMs of orthogonal polarization states (transverse electric and transverse magnetic). By carefully exciting WGMs inside this polymeric spheroidal cavity using another micron-sized optical fiber taper, positioned in evanescent mode vicinity to the resonation cavity along its meridian circumference, we can accurately monitor the spectral shift of orthogonal polarization WGMs of the same modal order under varying strain conditions.

Each WGM localized into a spherical resonator is defined by the radial (q), angular (l), and azimuthal (m) modal numbers, as well as its polarization state with respect to the plane vertical to the equator of the resonator.[14,18] The modal index q gives a number field maxima in the radial function of the electric field intensity, l represents the number of waves in a circular orbit,

DOI: 10.1021/acsomega.7b01409
ACS Omega 2017, 2, 9127−9135

and m is the azimuthal modal index ($-l < m < l$), describing the extension of the electrical field along the polar meridian of the microspheroid resonator. In homogeneous spheres, the optical modes are described as TE or TM, with the electric field being parallel or perpendicular to the resonator surface, respectively (Figure 1a).

For WGMs with $q = 1$, exhibiting intrinsically higher quality Q-factor, the spectral position of resonant wavelengths of the two modes in the equatorial area of a spherical cavity is given by[18,19]

$$\lambda_{TE} = 2\pi n_s r\left(\nu + 1.8557\,\nu^{1/3} - \frac{n}{\sqrt{n^2-1}} + 1.0331\,\nu^{-1/3} - \frac{0.6186\,n^3}{(n^2-1)^{3/2}}\,\nu^{-2/3} + O(\nu^{-1})\right)^{-1} \quad (1)$$

$$\lambda_{TM} = 2\pi n_s r\left(\nu + 1.8557\,\nu^{1/3} - \frac{1}{n\sqrt{n^2-1}} + 1.0331\,\nu^{-1/3} - \frac{1.8557\left(n^4-\frac{2}{3}\right)}{n^3(n^2-1)^{3/2}}\,\nu^{-2/3} + O(\nu^{-1})\right)^{-1} \quad (2)$$

where n_s is the refractive index of the resonator, r is the radius, $n = n_s/n_e$ is the refractive index contrast between the resonator and the outer environment (n_e), and $\nu = l + \frac{1}{2}$. The choice of $q = 1$ radial modes is also prompted by our principal interest in studying photoelastic changes, as close to the sample surface as possible. Using the comb of TE peaks (eq 1) with is $n_s = n_{PS}$ at the IR frequencies extrapolated from the dispersion relation,[20] we estimate the effective r for a modal number ν (l). Because the glassy PS spheroid can possess an inherent birefringence due to its fabrication, the value of n_{TM} entering eq 2 can deviate from $n_{TE} = n_{PS}$. The former can be obtained from eq 2 using fixed r and ν values already evaluated for the other polarization. We note that the WGM cavities (inset to Figure 1) deviate from of a spheroidal shape but exhibit small eccentricities ($\leq$0.2). However, we consider that the eccentricity affects absolute WGM wavelength allocation, but not birefringence (eq 4 below).

Through the controlled stretching of the optical fiber taper supporting the PS spheroid (inset to Figure 1), a spectral shift is induced to the WGM resonances. This can arise mainly from changes in both the refractive index and the radius of the spheroid, assuming unaltered modal order (assumption valid for small strains applied) and negligible eccentricity changes.[6a] The spectral shifts in the TE and TM WGMs emerging from the strain application are ascribed to both resonator radius (Δr) and refractive index ($\Delta n_{TE,\,TM}$) alterations,[6a] following the simple differential form

$$\frac{\Delta\lambda_{TE}}{\lambda_{TE}} = \frac{\Delta r}{r} + \frac{\Delta n_{TE}}{n_{TE}} \text{ and } \frac{\Delta\lambda_{TM}}{\lambda_{TM}} = \frac{\Delta r}{r} + \frac{\Delta n_{TM}}{n_{TM}} \quad (3)$$

where $\Delta\lambda_{TX} \equiv \lambda_{TX}(\varepsilon) - \lambda_{TX}(0)$ and $\Delta n_{TX} \equiv n_{TX}(\varepsilon) - n_{TX}(0)$ (index X stands for either E or M) and ε denotes the applied strain. Elimination of the radius dependence leads to a straightforward relation

$$\Delta n_{strain} = \Delta n_{TE} - \Delta n_{TM} = \left(\frac{\Delta\lambda_{TE}}{\lambda_{TE}} - \frac{\Delta\lambda_{TM}}{\lambda_{TM}}\right)n_s \quad (4)$$

under the assumption that $n_s \approx n_{TX}$. By employing eq 4, the differential shift between the two polarizations was employed to calculate change in birefringence, which was induced by applied strain. eq 4 indicates that under the condition of small applied strains, the method followed herein is independent of the modal order of the WGM notch investigated. Because our sample exhibits a spherical symmetry, the strain-induced refractive index changes per polarization component in spherical coordinates are described by the following relationships[6a]

$$\Delta n_{TE} = -\frac{n_s^3}{2}(p_2 S_{rr} + p_1 S_{\theta\theta} + p_2 S_{\varphi\varphi})$$

$$\Delta n_{TM} = -\frac{n_s^3}{2}(p_1 S_{rr} + p_2 S_{\theta\theta} + p_2 S_{\varphi\varphi}) \quad (5a,b)$$

where S_r, S_θ, and S_ϕ are the strain components per coordinate and p_1 and p_2 are the strain-optical constants of polystyrene. By combining eqs 4 and 5a,b, we get

$$\frac{\Delta n_{strain}}{n_s} = \frac{n_s^2}{2}(p_2 - p_1)(S_{\theta\theta} - S_{rr}) \quad (6)$$

To evaluate the strain-optical coefficient k' of an optical material, the strain-induced birefringence Δn_{strain} is directly correlated with the applied strain, ε, through the simple strain-optical law

$$k' = \frac{\Delta n_{strain}}{(S_{\theta\theta} - S_{rr})} \quad (7)$$

where $(S_{\theta\theta} - S_{rr}) = A\varepsilon$; A is a dimensionless multiplicative factor emerging from the finite-element strain distribution calculations for the strain components S_{rr} and $S_{\theta\theta}$ (see Figure 2). Although the strain ε applied on the two ends of the standard telecom optical fiber is precisely measured using the experimental apparatus, its transmission to the equatorial circumference of the polystyrene spheroid into the components S_{rr} and $S_{\theta\theta}$ depends on the shape of the spheroid and the geometry of the tapered optical fiber.[21]

We model the tapered optical fiber as two cones connected through a thin silica glass fiber, as shown in the left-hand diagram of Figure 2. The results are based on a finite-element numerical method. The S_{zz} component of the strain profile, as propagated in the region of the spheroid, and the relationship of the strain difference to the external applied strain are shown in the middle and lower insets of Figure 2, respectively. From the linear relation between $S_{\theta\theta} - S_{rr}$ and the strain ε_f applied to the fork (Figure 2), the slope A factor is valued as 1.2 for the polystyrene spheroids with radius of ~15 μm. The stress-optical coefficient $k = n_s^3\frac{1+\nu}{2E}(p_2 - p_1)$ [22] is related to the strain-optical coefficient, $k' = (n_s^3/2)(p_2 - p_1)$ (eqs 6 and 7) by

$$k = k'\frac{1+\nu}{E} \quad (8)$$

where ν is Poisson's ratio and E is Young's modulus. The sign of k' defines the relative magnitude of the two strain-optical

DOI: 10.1021/acsomega.7b01409
ACS Omega 2017, 2, 9127−9135

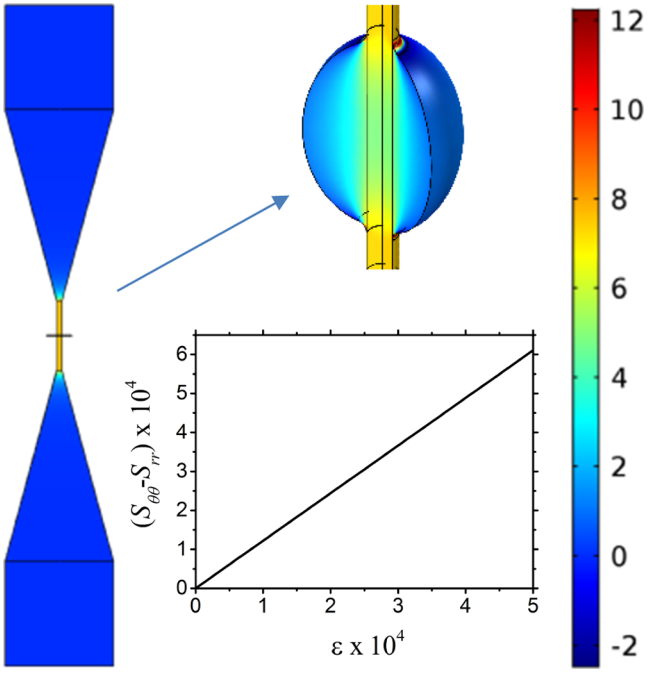

Figure 2. Ratio of the S_{zz} component of the strain profile normalized to the externally applied strain, ε (see color bar). In the left-hand side, the whole structure is depicted with an aspect ratio of horizontal to vertical axis 50:1 for visualization purposes. The spheroidal particle (shown as a line in the center of the left-hand diagram) is shown in the middle with an aspect ratio of 1:1. In the inset, we show the linear dependence of the strain difference $S_{\theta\theta} - S_{rr}$ as a function of ε.

constants, i.e., $k' < 0$, if $p_2 - p_1 < 0$ and vice versa. It is worth noting that the polarized and depolarized light-scattering intensities, respectively, depend on p_2^2 and $(p_2 - p_1)^2$, rendering any information on the sign of $p_2 - p_1$ ambiguous.[23]

RESULTS AND DISCUSSION

Polystyrene, a readily vitrified amorphous polymer, resides in the glassy state at ambient conditions. The two PS samples with low (PS2k, T_g = 336 K) and high (PS50k, T_g = 383 K) molecular weights were selected on the account of their different glass transition temperatures, T_g (Figure S1). Hence, the two samples represent different quenches at room temperature that could cause different local packing and segmental orientation. Yet, birefringence turns out to be a very sensitive probe of orientation fluctuations, and refractive index changes in the WGMs cavity are sensitively manifested in differential shifts between the corresponding TE and TM resonant modes, as already mentioned. The polarization-resolved transmission spectra recorded with the tapered fiber in contact with the PS spheroid (Figure 1) using PS50k are shown in Figure 3a. The sharp and distinct WGM's spectral notches for TE and TM polarization of different modal number l indicate a high-quality (Q-TE_{89} = 2.3 × 10^4) spheroidal cavity.

From the WGM spectra of the unstrained spheroid, the inherent birefringence, $\Delta n_0 = n_{TE} - n_{TM}$, for the system was estimated (eqs 1 and 2) to be about -3×10^{-4}. The attribution of modal order l for the data of Figure 3 for the PS50k sample (as well as for the PS2k and bidisperse samples presented afterward) was assumed for radial order q = 1. Attempts to fit the same data using higher radial order modes (q = 2)[24] led to abnormally high inherent birefringence values ($\Delta n_0 \sim -3.5 \times 10^{-3}$), not justified by the sample preparation process (slow annealing above T_g), as well as by the strain birefringence measurements presented below. The estimation of inherent birefringence is an important first result, revealing the initial stress state of the PS microspheroid cavity while depicting that the axial load with refractive index is larger in the direction of the TM, i.e., normal to the spheroid. The inherent birefringence for the PS2kDa microresonator, $\Delta n_0 = -2 \times 10^{-4}$, is found to be also negative with somewhat smaller absolute value than for PS50k.[25] Residual stresses ($\sim\Delta n_0/k$) in the nonequilibrium glassy state are not unexpected,[16] but their reliable assessment allows for an additional structural characterization. Internal stresses in glassy polymers can arise from trapped conformational states (segmental orientation) and packing (density anisotropy) changes.[26] In either case, the finite negative Δn_0 in the glassy PS implies that the polarizable phenyl side groups should be preferentially aligned normal to the spheroid surface.[15b] This frozen-in polymer conformation is more pronounced in the PS50k (high T_g) and probably reflects different thermal experience of the surface relatively to the

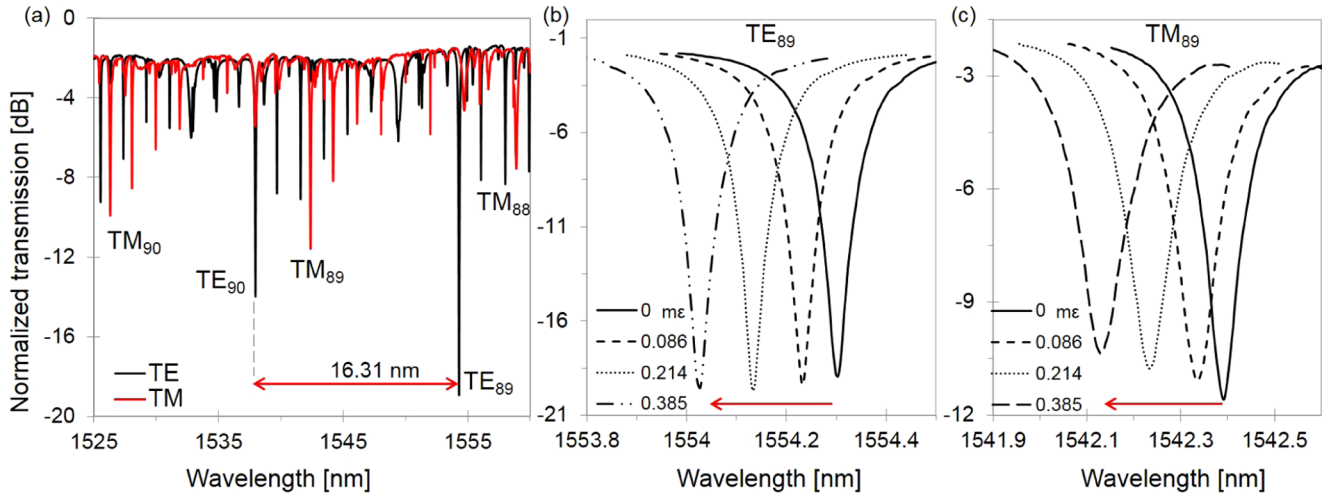

Figure 3. (a) Measured WGM's signal normalized with the taper transmission for the WGMs with TE (black) and TM (red lines) polarization along the spacing (FSR = 16.31 nm) of two adjacent TE modes in the case of PS50k. The blue shift of the resonance wavelength for the TE (b) and TM (c) polarizations (angular number l = 89) with increasing applied strain ε.

DOI: 10.1021/acsomega.7b01409
ACS Omega 2017, 2, 9127−9135

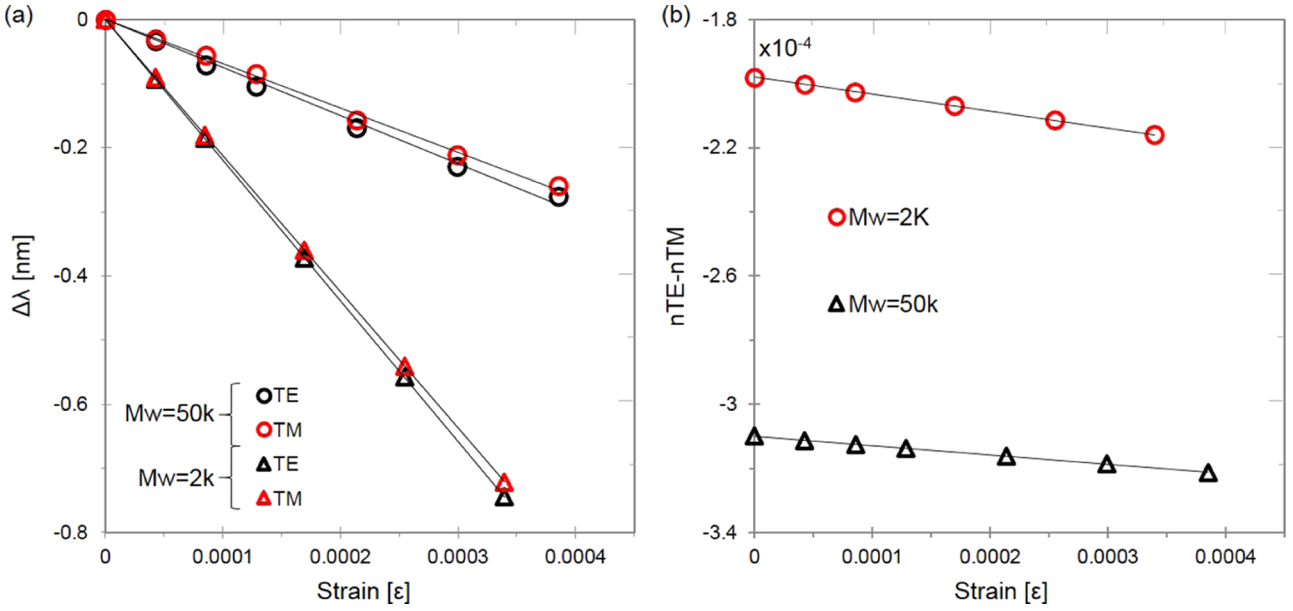

Figure 4. (a) WGM resonant wavelength shift for TE and TM modes and (b) strain-induced optical birefringence (eq 4) as a function of applied strain ε for PS2k and PS50k with molecular weight of 2 and 50 kDa, respectively. The spectral resolution applied in the above measurements is 10 pm; thus, error bars are smaller than the size of the actual symbols used.

center of the spheroid[27] with impact in the thin-film technology.[28]

The wavelength shift of the WGMs notches for both polarizations and PS2k and PS50k cavities exhibits a linear dependency upon the strains applied (see Figure 4a); this is also related to the minimum strain load (0.04%) applied. Strains applied to the positioning fork up to 3.85×10^{-4} for the PS50k spheroid produced wavelength shifts (Figure 3b,c) of the WGM with the modal order $l = 89$ up to 0.28 nm for the TE polarization and 0.26 nm for the TM mode (Methods). Upon strain of the PS50k and PS2k cavities, both TE and TM polarization WGMs exhibit excellent spectral shifting capabilities, preserving well-defined modal shapes without perturbation of the excitation conditions. The average slope, $\Delta\lambda/\delta\varepsilon$ (=2.18 and 0.7 nm/mε), emerging from both the TE and TM components is about 3 times steeper for PS2k microspheroid (Figure 4a) while considering similar sphere sizes/shapes and modal orders. According to eq 3, the value $\Delta\lambda/\lambda$ ($=-1.4 \times 10^{-4}$, for PS2k) is controlled by the contributions of Δn and Δr, both being material characteristic. From the FEM calculations, $\Delta r/r = -0.87\ m\varepsilon$, thus an average figure for $\Delta n_{strain}/n_s = -0.53\ m\varepsilon$. Alternatively, the average $\Delta n_{strain}/n_s$ can be also estimated by adding eqs 5a,b for both polarizations while accounting for the strain profile (see Figure 2) $S_{rr} = -0.12\ m\varepsilon$, $S_{\varphi\varphi} = -0.87\ m\varepsilon$, $S_{\theta\theta} = 1.10\ m\varepsilon$; thus, $\Delta n_{strain}/n_s = -(n_s^2/2)(0.49p_1 - 0.38p_2)m\varepsilon$ is negative with $p_1 > p_2$. Similar calculations for the case of PS50K will lead to a positive average $\Delta n_{strain}/n$. However, the different slopes for the two PS spheroids depend on both $\Delta r/r$ and $\Delta n_{strain}/n_s$, which are determined by the local elastic and strain-optical constants, respectively.

The slope of the curves in Figure 4b, divided by the multiplicative parameter A (eq 7), yields the strain-optical coefficient, k'. The strain-optical coefficients evaluated for the 50 and 2 kDa samples unexpectedly assume negative values −0.024 and −0.055. We recall that the reported k' for bulk PS in the glassy state is positive.[15a] Using the experimental values 0.34 for Poisson's ratio and 3.8 GPa for the Young modulus, as obtained from Brillouin light-scattering spectra (Figure S2), the stress-optical coefficients k (eq 8) amounts to −8.66 Br for PS50k and −19.5 Br for the PS2k spheroids. Although the absolute value of these stress-optical coefficients exhibit a good agreement with those reported for bulk, glassy PS samples,[15a,29] their negative sign implies a chain conformation similar to that of stretched PS melt. In the rubbery state, above T_g, it is well established that $k' < 0$ due to the contribution of chain conformation and preferential orientation of the phenyl side groups normal to the stretching direction.[15b] A similar sign change in k' in the glassy state was reported for thin PS films also attributed to the alignment of the phenyl groups of the PS chains vertically to the axis of strain application.[30] An additional notable point of our investigation is that both the initial birefringence of the PS spheroids and the stress-optical coefficients for the examined molecular weights are negative, contrary to the results obtained for bulk samples. Because the present technique probes a few microns thick shell overlapping with the modal volume of the WGM (see Figure 1), this disparity with the bulk could imply different segmental alignment properties close to the surface than in the interior of the spheroids.

Apart from the sign, the value of k' (or k) seems to also depend on the chain length, or T_g, as suggested by the larger absolute value of k for PS50k. It could also be an inherent property of a still poorly understood vitrification of amorphous polymers. For example, k turns from positive to negative for a glassy random copolymers of polystyrene with acrylonitrile[15b] and methylmethacrylate,[31] poly(styrene-*co*-acrylonitrile) when the PS composition drops beyond a certain composition about 70%,[31] which was again assigned to the phenyl ring side-group conformation. For the present study, a straightforward experiment is a bidisperse PS2k/PS50k blend with the T_g very similar to the PS2k component. A polystyrene spheroid was accordingly prepared by mixing equal moles of PS50k and PS2k, resulting in a symmetric polymer mixture with regard the monomer composition, but very rich in short chains (about 25 times more PS2k chains). Due to the same chemical monomer,

DOI: 10.1021/acsomega.7b01409
ACS Omega 2017, 2, 9127−9135

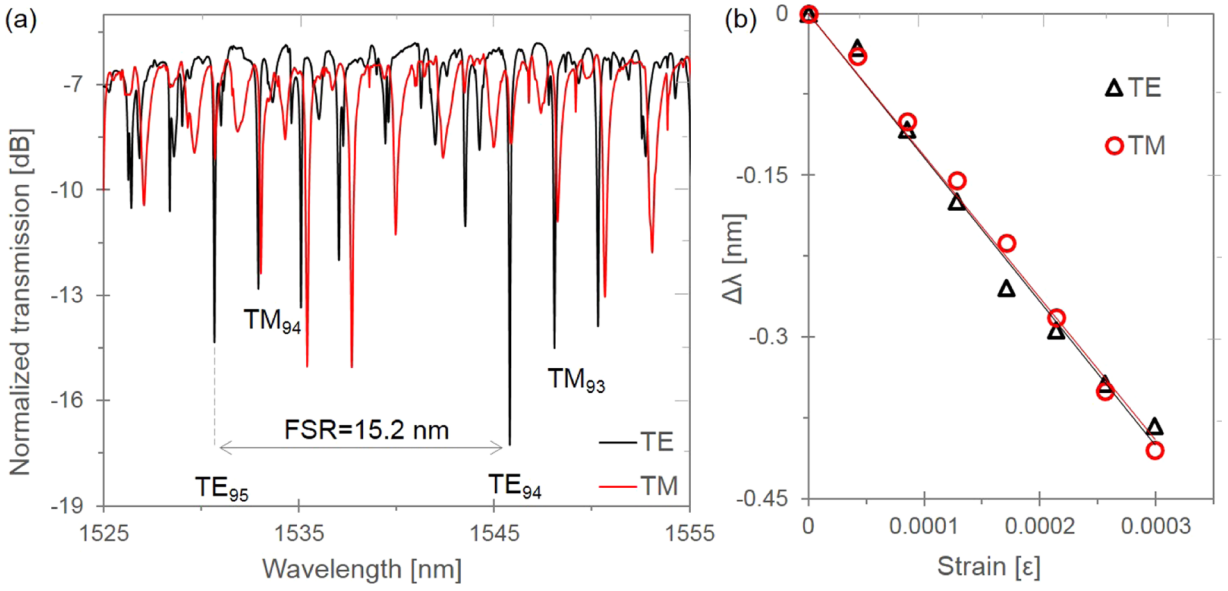

Figure 5. (a) Measured WGM's signal, normalized with the taper transmission for the WGMs with TE (black) and TM (red lines) polarization along the spacing (FSR = 15.2 nm) of two adjacent TE and TM modes. (b) WGM resonant wavelength shift for TE and TM mode in the case of the spheroid with symmetric PS2k/PS50k.

the mixing is purely entropic in spite of small differences in the density of the two constituent PS and hence refractive indices. The bidisperse glass exhibits the same T_g (=336 K) as the PS2k as a result of the plasticization effect due to the significant fraction of free chain ends (in PS2k); this is verified by DSC (Figure S3). The WGM spectra for both polarization components obtained from a 32 μm diameter bidisperse spheroid are presented in Figure 5a.

A first inspection of the polarization-resolved spectra of this bidisperse resonator shows that the WGM resonances for both polarizations are of broader bandwidth (Q-TE_{94} $\sim$ 1.4×10^4 and Q-TM_{94} $\sim$ 0.9×10^4) compared to those of the monodisperse samples, thus, of lower Q-factor. This broadening behavior is more prominent for the TM polarization modes, being perpendicular to the strain application direction. Even for an ideally homogeneous resonator with negligible composition fluctuations, the small refractive index mismatch ($\sim 1.5 \times 10^{-2}$ between PS2k and PS50k) is still high enough to induce significant phase changes in the WGM confined light, resulting in modal broadening and/or polarization cross-coupling. In contrast to the monodisperse spheroids (Figure 4a), the shifts λ_{TE} and λ_{TM} (Figure 5b) exhibit a nonmonotonic behavior with alternating slopes from negative to positive birefringence, rendering a reliable estimation of total birefringence, $n_{TE} - n_{TM}$, unlike Figure 4b, ambiguous. Nevertheless, the average slope for both polarization modes $\Delta\lambda/\delta\varepsilon$ ($\sim$1 nm/mε) versus strain of the bidisperse spheroid (Figure 5b) rests between those of the PS2k and PS50k, but is closer to the PS50k.

A possible explanation of this polarization-dependent finding maybe related to the optical inhomogeneities in the surface region (Figure 1) because the thermomechanical properties of the bulk bidisperse symmetric PS mixture remain robust. Both the T_g of the PS2k/PS50k (Figure S3) is almost identical to PS2k and the sound velocities c_L in the mixture and the two components (Figure S4) are experimentally the same. The latter conforms to the picture of the ideal mixture with negligible composition inhomogeneities. Seemingly, this bulk behavior does not hold near the surface, where the spatial fluctuations of the refractive index due to the phenyl ring orientation are present. The role of different component dynamics[31,32] might play a role as the mixture enters to the glassy state through the solvent evaporation.

Based on eq 6, the strain-induced optical effects can impact the strain-optical constants of glassy polystyrene that can be easily revealed by changes in the depolarization of the inelastic light scattering (Figure S5). The origin of abnormal photoelastic behavior of the bidisperse resonator can be manifold and related to both the material properties of the mixture and the WGM light localization physics. Nanodomain inhomogeneities can lead to modal crossing induced by the excitation of transverse modes of different polar mode order m into the polystyrene spheroid[33] and cross-polarization coupling effects,[34] in addition to the modal splitting. The application of strain into the spheroid can amplify such type of interaction, resulting in anomalous modal birefringence, which, in turn, is erroneously manifested as abnormal material birefringence and photoelastic behavior. Therefore, the data obtained for the bidisperse polystyrene spheroid are useful for investigating the sensitivity of the method on photoelastic parameters of the material on micro- and nanoscale. Studies are ongoing for illustrating the origin of the photoelastic behavior of the bidisperse polystyrene WGM spheroid resonator, whereas efforts are focused on further expanding the metrological capabilities of the method.

CONCLUSIONS

We introduced a new method for the precise measurement of the photoelastic properties of glassy polymers (polystyrene) harnessing microspheroid resonators attached on tapered optical fibers. Whispering gallery modes (WGMs) were efficiently excited in the microresonator scheme and showed excellent linear spectral shift with the strain applied. The differential wavelength shift between TE and TM modes allowed for accurate monitoring of changes in the material birefringence of the spheroid that are associated with the strain-

DOI: 10.1021/acsomega.7b01409
ACS Omega 2017, 2, 9127−9135

induced weak stresses. The obtained strain- and stress-optical coefficients revealed a negative photoelastic behavior for two monodisperse (2 and 50 kDa) microspheroid resonators, contrary to the bulk polystyrene. This particular photoelastic behavior with phenyl group oriented vertically to the axis of strain application indicates a polystyrene scale-dependent segmental alignment.

For a symmetric bidisperse PS spheroid (50 kDa/2 kDa) possessing the same glass transition temperature as PS2k, the method revealed a substantially different segmental orientation than in the two monodisperse analogues. The spectral results depicted that WGM resonating cavities, even of modest Q-factors ($\sim 10^4$), are extremely sensitive to the phase retardations induced by refractive index fluctuations in the nanoscale. Effects such as modal broadening, cross-coupling take place and are further amplified by the application of strain load, transducing chain orientation effects of the intermixed monomers to abnormal optical birefringence behavior. Notably, the distinct segmental PS polarizability can selectively affect the polarization component of the WGMs that are aligned with respect to polarization anisotropy.[35] The above new metrological findings render polarization resolved WGM resonation in strain applied polymeric cavities, a promising tool for the study of orientation properties of macromolecules systems. Further investigations are directed to the study of the unique elasto-optic behavior of fiber structures made from natural silks using WGM resonation photoelastic spectroscopy.

METHODS

Whispering Gallery Mode (WGM) Excitation and Spheroid Preparation. Fiber tapers were fabricated from a single-mode fiber SM28 with Vytran GPX-3000 optical fiber fuser while being positioned on an adjustable opening Invar fork for controllably applying strain on them. The strain was applied through deforming the fork using a differential micrometric vernier with 1 μm traveling accuracy. The applied strain ε was directly measured through the vernier scale and also confirmed by the attachment of an optical fiber Bragg grating parallel to the optical fiber taper supported on the polystyrene spheroid.

Polystyrene of two molecular weights was used in the experiments: 50 and 2 kDa molecular weights were chosen, due to their distinct T_g points, more significantly for their distinct segmental and chain orientation with respect to the phenyl group of the PS matrix that dominates their corresponding rheological and stress-optical properties. To investigate the stress-optical properties of a system with more complex segmental structure, an equimolar mixture of the 50 and 2 kDa molecular weights was also prepared. Using a syringe, a PS/toluene solution with concentration ~0.1% for all molecular weights tested was dropped onto an optical fiber taper (waist diameter ~6.0 μm). Dilute solutions below the overlap concentration are necessary to avoid fast solidification of the drop. The solvent was removed under vacuum at $T \sim T_g + 25$ (glass transition T_g(2k) = 336 K, T_g(50k) = 382 K, T_g(2k/50k) = 383 K) for 6 h and subsequently the wrapped PS drop was cooled down for 24 h, leading to the formation of low-eccentricity spheroid cavities with a typical diameter of 30 μm (Figure 1 inset). For comparison reasons, polystyrene microspheroids "as-fabricated" after the first casting and then after the controlled annealing processes described above are provided in Figure S6.

Broadband superluminescent laser diode (SLD) launched into a second fiber taper with a waist diameter of 2.5 μm, placed perpendicular to the first one in the equatorial region of the sphere, was used to excite WGMs (Figure 1). Transmission spectra for TE and TM modes are separately recorded with optical spectrum analyzer (OSA), utilizing polarizing ZING fiber from Fibercore, at the fiber taper output and a spectral resolution of 0.01 nm. For the strain measurements, both fiber taper ends were fixed on opposite arms of a metal fork, and arms opening with micrometer screw allowed for controllable fiber elongation. The initial tapered fiber length was 30 mm, whereas the maximum length increase used in experiment was 11.55 μm, corresponding to a strain ε of 0.385×10^{-3} or 0.385 mε. The size of the polymer spheroid was measured using an optical stereoscope with a resolution limit of ~1 μm. The optical fiber taper was placed in contact with the spheroid, and WGM excitation was achieved under different strain conditions. For excluding creeping effects between the supporting optical fiber taper and the PS spheroid, spectral measurements were repeated after strain relaxation, where no spectral hysteresis of the WGMs was observed.

Brillouin Light Scattering (BLS). Polarized (VV) and depolarized (VH) BLS spectra were recorded by a tandem six-pass Fabry–Perot interferometer at different phonon wavelengths. The longitudinal c_L and transverse c_T sound velocities (in the case of solids) are obtained from the polarized (VV) and depolarized (VH) BLS spectra, respectively. V(V, h) stands for laser polarization vertically, V, and scattered light being either vertically (v) or horizontally (h) relatively to the scattered plane (the scattered plane is defined by the wave vectors of the laser and the scattered light). BLS measures the sound velocity for the longitudinal and transverse phonons through the inelastic light scattering by the propagation of thermally excited phonon in the material. In homogeneous materials with linear acoustic behavior, the frequency, $f = cq/(2\pi)$, is proportional to the magnitude of the phonon wave vector, q, defined by the scattering geometry. The longitudinal c_L and transverse c_T sound velocity (in the case of solids) are obtained from the polarized (VV) and depolarized (VH) BLS spectra, respectively (Figure S2). V(V, h) stands for laser polarization vertically, V, and scattered light being either vertically (v) or horizontally (h) relatively to the scattered plane (the scattered plane is defined by the wave vectors of the laser and the scattered light). The access to both longitudinal $M = \rho c_L^2$ and shear $G = \rho c_T^2$ moduli with c_L = (2370 ± 20) m/s and c_T = (1170 ± 10) m/s allows the estimation of Young's modulus, $E = 2G(1 + \nu)$, where ρ (=1.04 g/cm^3 for PS) is the density and $\nu = (c_L^2 - 2c_T^2)/[2(c_L^2 - 2c_T^2)] = 0.34$, is Poisson's ratio. Hence, G = 1.4 GPa and E = 3.8 GPa.

ASSOCIATED CONTENT

Supporting Information

The Supporting Information is available free of charge on the ACS Publications website at DOI: 10.1021/acsomega.7b01409.

Molecular weight dependence of the glass transition temperature, T_g, obtained from differential thermal calorimetry (DSC) for five PS samples; polarized (VV) and depolarized (VH) Brillouin light-scattering spectra of PS2k; DSC traces for PS2k and the mixture PS2k and PS50k with symmetric monomer composition; longitudinal and transverse sound velocities versus temperature in the symmetric PS2k/PS50k mixture and

DOI: 10.1021/acsomega.7b01409
ACS Omega 2017, 2, 9127–9135

monodisperse PS2k; polarized and depolarized BLS spectra of PS2k and PS20k; polystyrene drops casted onto optical fiber tapers before and after annealing process (PDF)

AUTHOR INFORMATION

Corresponding Authors

*E-mail: pissas@iesl.forth.gr.

*E-mail: fytas@mpip-mainz.mpg.de.

ORCID

Stavros Pissadakis: 0000-0002-4842-1328

Notes

The authors declare no competing financial interest.

ACKNOWLEDGMENTS

ARISTEIA, cod. 285 SophoX and ERC Smartphon Nr. 694977. S.P. acknowledges financial support from ACTPHAST (Grant Agreement No. 619205), H2020 RESPICESME (Grant Agreement No. 687961), and H2020 Laserlab Europe (EC-GA 654148). G.G. acknowledges financial support from EPSRC Projects EP/M027791/1 and EP/L02263X/1 (EP/M008576/1).

REFERENCES

(1) (a) Noto, M.; Keng, D.; Teraoka, I.; Arnold, S. Detection of Protein Orientation on the Silica Microsphere Surface Using Transverse Electric/Transverse Magnetic Whispering Gallery Modes. *Biophys. J.* **2007**, *92*, 4466−4472. (b) Hanumegowda, N. M.; Stica, C. J.; Patel, B. C.; White, I.; Fan, X. Refractometric sensors based on microsphere resonators. *Appl. Phys. Lett.* **2005**, *87*, No. 201107. (c) Foreman, M. R.; Swaim, J. D.; Vollmer, F. Whispering gallery mode sensors. *Adv. Opt. Photonics* **2015**, *7*, 168−240.

(2) Cai, M.; Painter, O.; Vahala, K. J.; Sercel, P. C. Fiber-coupled microsphere laser. *Opt. Lett.* **2000**, *25*, 1430−1432.

(3) von Klitzing, W.; Long, R.; Ilchenko, V. S.; Hare, J.; Lefèvre-Seguin, V. Frequency tuning of the whispering-gallery modes of silica microspheres for cavity quantum electrodynamics and spectroscopy. *Opt. Lett.* **2001**, *26*, 166−168.

(4) (a) Li, Y.; Svitelskiy, O. V.; Maslov, A. V.; Carnegie, D.; Rafailov, E.; Astratov, V. N. Giant resonant light forces in microspherical photonics. *Light: Sci. Appl.* **2013**, *2*, No. e64. (b) Ilchenko, V. S.; Bennett, A. M.; Santini, P.; Savchenkov, A. A.; Matsko, A. B.; Maleki, L. Whispering gallery mode diamond resonator. *Opt. Lett.* **2013**, *38*, 4320−4323.

(5) (a) Kosma, K.; Zito, G.; Schuster, K.; Pissadakis, S. Whispering gallery mode microsphere resonator integrated inside a micro-structured optical fiber. *Opt. Lett.* **2013**, *38*, 1301−1303. (b) François, A.; Riesen, N.; Ji, H.; Shahraam Afshar, V.; Monro, T. M. Polymer based whispering gallery mode laser for biosensing applications. *Appl. Phys. Lett.* **2015**, *106*, No. 031104.

(6) (a) Ilchenko, V. S.; Volikov, P. S.; Velichansky, V. L.; Treussart, F.; Lefèvre-Seguin, V.; Raimond, J. M.; Haroche, S. Strain-tunable high-Q optical microsphere resonator. *Appl. Opt.* **1998**, *145*, 86−90. (b) Ioppolo, T.; Kozhevnikov, M.; Stepaniuk, V.; Ötügen, M. V.; Sheverev, V. Micro-optical force sensor concept based on whispering gallery mode resonators. *Appl. Opt.* **2008**, *47*, 3009−3014. (c) Dinyari, K. N.; Barbour, R. J.; Golter, D. A.; Wang, H. Mechanical tuning of whispering gallery modes over a 0.5 THz tuning range with MHz resolution in a silica microsphere at cryogenic temperatures. *Opt. Express* **2011**, *19*, 17966−17972. (d) Roselló-Mechó, X.; Delgado-Pinar, M.; Díez, A.; Andrés, M. V. Measurement of Pockels' coefficients and demonstration of the anisotropy of the elasto-optic effect in optical fibers under axial strain. *Opt. Lett.* **2016**, *41*, 2934−2937.

(7) Ali, A. R.; Ioppolo, T.; Ötügen, V.; Christensen, M.; MacFarlane, D. Photonic electric field sensor based on polymeric microspheres. *J. Polym. Sci., Part B: Polym. Phys.* **2014**, *52*, 276−279.

(8) Ediger, M. D.; Forrest, J. A. Dynamics near Free Surfaces and the Glass Transition in Thin Polymer Films: A View to the Future. *Macromolecules* **2014**, *47*, 471−478.

(9) Fakhraai, Z.; Forrest, J. A. Measuring the Surface Dynamics of Glassy Polymers. *Science* **2008**, *319*, 600.

(10) Wagner, H. P.; Schmitzer, H.; Lutti, J.; Borri, P.; Langbein, W. Effects of uniaxial pressure on polar whispering gallery modes in microspheres. *J. Appl. Phys.* **2013**, *113*, No. 243101.

(11) (a) Dong, C.-H.; He, L.; Xiao, Y.-F.; Gaddam, V. R.; Ozdemir, S. K.; Han, Z.-F.; Guo, G.-C.; Yang, L. Fabrication of high-Q polydimethylsiloxane optical microspheres for thermal sensing. *Appl. Phys. Lett.* **2009**, *94*, No. 231119. (b) Madugani, R.; Yang, Y.; Ward, J. M.; Riordan, J. D.; Coppola, S.; Vespini, V.; Grilli, S.; Finizio, A.; Ferraro, P.; Nic Chormaic, S. Terahertz tuning of whispering gallery modes in a PDMS stand-alone, stretchable microsphere. *Opt. Lett.* **2012**, *37*, 4762−4764.

(12) Kavungal, V.; Mallik, A. K.; Farrell, G.; Wu, Q.; Semenova, Y. Strain-induced spectral tuning of the whispering gallery modes in a cylindrical micro-resonator formed by a polymer optical fiber. *Appl. Opt.* **2017**, *56*, 1339−1345.

(13) Nguyen, N. Q.; Gupta, N.; Ioppolo, T.; Ötügen, M. V. Whispering gallery mode-based micro-optical sensors for structural health monitoring of composite materials. *J. Mater. Sci.* **2009**, *44*, 1560−1571.

(14) Matsko, A. B.; Ilchenko, V. S. Optical resonators with whispering-gallery modes-part I: basics. *IEEE J. Sel. Top. Quantum Electron.* **2006**, *12*, 3−14.

(15) (a) Rudd, J. F.; Gurnee, E. F. Photoelastic Properties of Polystyrene in the Glassy State. II. Effect of Temperature. *J. Appl. Phys.* **1957**, *28*, 1096−1100. (b) Takahashi, S.; Saito, H. Conformational Change of Phenyl Ring Side Group during Stress Relaxation in Glassy Poly(styrene-co-acrylonitrile). *Macromolecules* **2004**, *37*, 1062−1066.

(16) Tagaya, A.; Koike, Y. Compensation and control of the birefringence of polymers for photonics. *Polym. J.* **2012**, *44*, 306−314.

(17) Harris, J. K. A photoelastic substrate technique for dynamic measurements of forces exerted by moving organisms. *J. Microsc.* **1978**, *114*, 219−228.

(18) Oraevsky, A. N. Whispering-gallery waves. *Quantum Electron.* **2002**, *32*, 377−400.

(19) Lam, C. C.; Leung, P. T.; Young, K. Explicit asymptotic formulas for the positions, widths, and strengths of resonances in Mie scattering. *J. Opt. Soc. Am. B* **1992**, *9*, 1585−1592.

(20) Sultanova, N.; Kasarova, S.; Nikolov, I. Dispersion Properties of Optical Polymers. *Acta Phys. Pol., A* **2009**, *116*, 585−587.

(21) Wang, X.; Li, W.; Chen, L.; Bao, X. Thermal and mechanical properties of tapered single mode fiber measured by OFDR and its application for high-sensitivity force measurement. *Opt. Express* **2012**, *20*, 14779−14788.

(22) (a) Primak, W.; Post, D. Photoelastic Constants of Vitreous Silica and Its Elastic Coefficient of Refractive Index. *J. Appl. Phys.* **1959**, *30*, 779−788. (b) Okamoto, K. *Fundamentals of Optical Waveguides*, 2nd ed.; Academic Press: Burlington, MA, 2006; pp 310−311.

(23) Manenkov, A. A.; Ritus, A. I. Determination of the elastic and elasto-optic constants and extinction coefficients of the laser glasses LGS-247-2, LGS-250-3, LGS-I, and KGSS-1621 by the Brillouin scattering technique. *Sov. J. Quantum Electron.* **1978**, *8*, 78.

(24) (a) Svitelskiy, O.; Li, Y.; Darafsheh, A.; Sumetsky, M.; Carnegie, D.; Rafailov, E.; Astratov, V. N. Fiber coupling to $BaTiO_3$ glass microspheres in an aqueous environment. *Opt. Lett.* **2011**, *36*, 2862−2864. (b) Mohd Nasir, M. N.; Senthil Murugan, G.; Zervas, M. N. Spectral cleaning and output modal transformations in whispering-gallery-mode microresonators. *J. Opt. Soc. Am. B* **2016**, *33*, 1963−1970.

(25) Leclerc, G.; Yelon, A. Birefringence measurements of thin dielectric films by the prism coupler method. *Appl. Opt.* **1984**, *23*, 2760−2762.

DOI: 10.1021/acsomega.7b01409
ACS Omega 2017, 2, 9127−9135

(26) Shimo, T.; Nagasawa, M. Stress and birefringence relaxations of noncrystalline linear polymer. *Macromolecules* **1992**, *25*, 5026−5029.
(27) McKenna, G. B. Mechanical rejuvenation in polymer glasses: fact or fallacy? *J. Phys.: Condens. Matter* **2003**, *15*, S737−S763.
(28) Reiter, G.; Hamieh, M.; Damman, P.; Sclavons, S.; Gabriele, S.; Vilmin, T.; Raphael, E. Residual stresses in thin polymer films cause rupture and dominate early stages of dewetting. *Nat. Mater.* **2005**, *4*, 754−758.
(29) Rudd, J. F.; Andrews, R. D. Photoelastic Properties of Polystyrene in the Glassy State. III. Styrene Derivatives and Copolymers. *J. Appl. Phys.* **1960**, *31*, 818−826.
(30) Ay, F.; Kocabas, A.; Kocabas, C.; Aydinli, A.; Agan, S. Prism coupling technique investigation of elasto-optical properties of thin polymer films. *J. Appl. Phys.* **2004**, *96*, 7147−7153.
(31) Ylitalo, C. M.; Kornfield, J. A.; Fuller, G. G.; Pearson, D. S. Molecular weight dependence of component dynamics in bidisperse melt rheology. *Macromolecules* **1991**, *24*, 749−758.
(32) Kanetakis, J.; Fytas, G.; Kremer, F.; Pakula, T. Segmental dynamics in homogeneous 1,4-polyisoprene-1,2-polybutadiene diblock copolymers. *Macromolecules* **1992**, *25*, 3484−3491.
(33) Attar, S. T.; Shuvayev, V.; Deych, L.; Martin, L. L.; Carmon, T. Level-crossing and modal structure in microdroplet resonators. *Opt. Express* **2016**, *24*, 13134−13141.
(34) Bianucci, P.; Fietz, C. R.; Robertson, J. W.; Shvets, G.; Shih, C.-K. Polarization conversion in a silica microsphere. *Opt. Express* **2007**, *15*, 7000−7005.
(35) Zhu, J.; Ozdemir, S. K.; Xiao, Y.-F.; Li, L.; He, L.; Chen, D.-R.; Yang, L. On-chip single nanoparticle detection and sizing by mode splitting in an ultrahigh-Q microresonator. *Nat. Photonics* **2010**, *4*, 46−49.

DOI: 10.1021/acsomega.7b01409
ACS Omega 2017, 2, 9127−9135